ASTRONOMY

The origin of RNA precursors on exoplanets

Paul B. Rimmer[1,2]*, Jianfeng Xu[2], Samantha J. Thompson[1], Ed Gillen[1], John D. Sutherland[2], Didier Queloz[1]

Given that the macromolecular building blocks of life were likely produced photochemically in the presence of ultraviolet (UV) light, we identify some general constraints on which stars produce sufficient UV for this photochemistry. We estimate how much light is needed for the UV photochemistry by experimentally measuring the rate constant for the UV chemistry ("light chemistry", needed for prebiotic synthesis) versus the rate constants for the bimolecular reactions that happen in the absence of the UV light ("dark chemistry"). We make these measurements for representative photochemical reactions involving SO_3^{2-} and HS^-. By balancing the rates for the light and dark chemistry, we delineate the "abiogenesis zones" around stars of different stellar types based on whether their UV fluxes are sufficient for building up this macromolecular prebiotic inventory. We find that the SO_3^{2-} light chemistry is rapid enough to build up the prebiotic inventory for stars hotter than K5 (4400 K). We show how the abiogenesis zone overlaps with the liquid water habitable zone. Stars cooler than K5 may also drive the formation of these building blocks if they are very active. The HS^- light chemistry is too slow to work even for early Earth.

INTRODUCTION

Dozens of exoplanets have been found within the liquid water habitable zones of their host stars (*1*–*4*). Living organisms could potentially thrive on the subset of these planets with stable atmospheres, but could life start on these planets in the first place? This question can, in principle, be answered in terms of whether the conditions necessary for life under a given scenario could be plausibly met on another planet, given what we know about that planet. We can delineate an abiogenesis zone, outside of which life is unlikely to have originated in the way the given scenario describes. We will focus on the photochemical scenarios presented by Patel *et al.* (*5*) and Xu *et al.* (*6*), which we find compelling because these are currently the only known prebiotically plausible chemical networks to selectively achieve high yields of nucleosides, amino acids, and lipid precursors from chemical initial conditions that are realistic for early Earth. Although these networks detail how the building blocks of life may have been formed, and not the method of their assembly, this first step is a necessary condition for life's origin (*7*).

It is fortuitous that the scenario we choose to investigate is connected to the light of the host star, the one thing we know best about any exoplanet system. We can connect the prebiotic chemistry to the stellar ultraviolet (UV) spectrum to determine whether these reactions can happen on rocky planets around other stars. Ranjan and Sasselov (*8*) have begun to explore whether life could arise photochemically on rocky planets around other stars, within the context of this scenario, and show that it is important to know the wavelength range over which this chemistry takes place. Experiments have shown that this critical wavelength range for these reactions is between 200 and 280 nm (*9*). A comparatively small amount of the UV light in this range is produced by ultracool stars, raising the question of whether the prebiotic inventory could ever arise on planets around these stars without the help of flares (*10*, *11*).

To assess where the Patel *et al.* (*5*) and Xu *et al.* (*6*) chemistry can realistically occur, we focus on key reactions along the seven-step pathway to form the pyrimidine nucleotide RNA precursors. This formation is driven by UV detachment of electrons from anions in solution, such as HS^- from H_2S (*5*) and SO_3^{2-} from SO_2 (*6*), in the presence of HCN. The HS^- reaction is representative of the Patel *et al.* (*5*) network, and the SO_3^{2-} reaction is representative of the Xu *et al.* (*6*) network, in the sense that each of the photochemical reactions take approximately the same amount of time under the exposure of the UV lamp used in both studies [supplementary materials of (*5*, *6*)]. Figure 1 shows the photochemical products, as well as inert adducts that build up when the light is absent. These inert adducts are sometimes useful for synthesizing amino acids but cannot lead to the formation of pyrimidine nucleotides. The rate constants for the photochemical reactions ("light chemistry") and the rate constants for the bimolecular reactions that take place in the absence of the UV lamp ("dark chemistry") can be used to estimate the yield of the light chemistry products. We define the abiogenesis zone as the zone in which a yield of 50% for the photochemical products is obtained, adopting the current UV activity as representative of the UV activity during the stellar lifetime and assuming a young Earth atmosphere.

The choice of a 50% yield is mandated by the "arithmetic demon," a well-known problem in synthetic chemistry involving many steps [for example, footnote 8 of (*12*)]. Because pyrimidine RNA precursors are needed building blocks for life in this scenario, and because the pathway to form these pyrimidines involves seven steps with similar photochemical rate constants, with three of these steps requiring two of these photochemical products reacting together, the final yield of the pyrimidines from a starting mixture of HCN and either SO_3^{2-} or HS^- will be the yields of each previous step multiplied together. A 10% yield at each stage will result in an overall pyrimidine yield of 10^{-8}%, a 30% yield for each step will result in a 6×10^{-4}% overall yield, and a 50% yield for each step will result in a 0.1% overall yield. Only the 50% yield per step is high enough for a robust prebiotic chemistry.

RESULTS

We now show our results from comparing the light chemistry and dark chemistry, to identify the environments in which the photochemical synthesis of pyrimidines is possible, for both SO_3^{2-} and HS^-. We found that the SO_3^{2-} dark chemistry was somewhat slower than the HS^- dark chemistry at low temperatures. In addition, the light chemistry is far

[1]Cavendish Astrophysics, University of Cambridge, JJ Thomson Avenue, Cambridge CB3 0HE, UK. [2]MRC Laboratory of Molecular Biology, Francis Crick Avenue, Cambridge CB2 0QH, UK.
*Corresponding author. Email: pbr27@cam.ac.uk

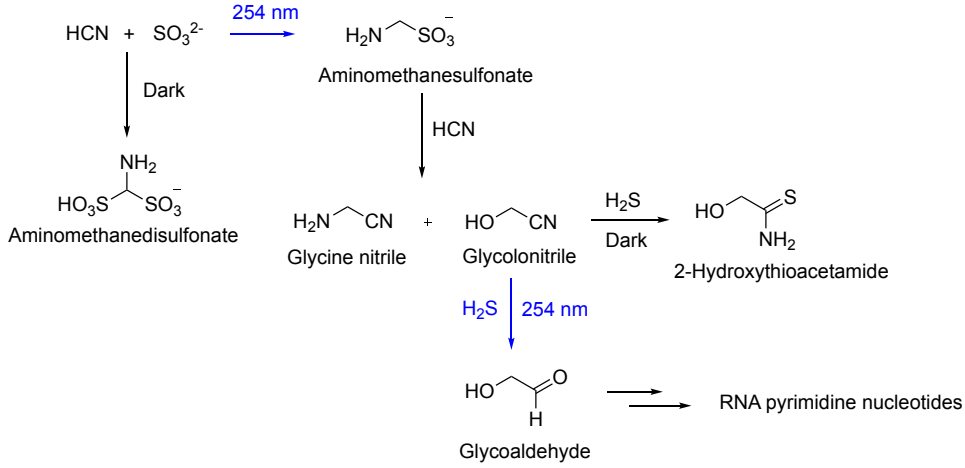

Fig. 1. Reaction scheme. The scheme of light and dark reactions we explore, considering two steps along the path to forming pyrimidines (RNA precursors): one with bisulfite (SO_3^{2-}) as the electron donor and the other with hydrogen sulfide (H_2S and HS^-) as the electron donor.

more rapid for SO_3^{2-}. The rate constants for the dark reactions, resulting in the adducts shown in Fig. 1, are

$$k_{\mathrm{add}}\left(SO_3^{2-} + \mathrm{HCN}\right) = (1.3 \pm 0.5) \times 10^8\ \mathrm{mol}^{-1}\ \mathrm{liter\ s}^{-1}\ e^{-(9500\pm106)\mathrm{K}/T} \quad (1)$$

$$k_{\mathrm{add}}(\mathrm{HS}^- + \mathrm{glycolonitrile}) = (2.0 \pm 0.7) \times 10^5\ \mathrm{mol}^{-1}\ \mathrm{liter\ s}^{-1}\ e^{-(7500\pm130)\mathrm{K}/T} \quad (2)$$

Under the assumption that the cross sections are constant between 200 and 280 nm [similar to Todd *et al.* (*9*)], we find that cross sections for SO_3^{2-} and HS^- to produce their respective photoproducts shown in Fig. 1 are

$$\sigma_{\mathrm{v}}\left(SO_3^{2-} + \mathrm{HCN}\right) = (1.5 \pm 0.3) \times 10^{-21}\ \mathrm{cm}^2 \quad (3)$$

$$\sigma_{\mathrm{v}}(\mathrm{HS}^- + \mathrm{glycolonitrile}) = (2.0 \pm 0.4) \times 10^{-23}\ \mathrm{cm}^2 \quad (4)$$

The dark chemistry is much slower at low temperatures. Because liquid water is a requirement for both the light and dark chemistry to proceed, we consider the best case for the light chemistry at a surface temperature of 0°C. In the case of SO_3^{2-}, the light chemistry and dark chemistry move at the same speed when the average actinic flux at the planet's surface between 200 and 280 nm is ~ 6×10^9 $\mathrm{cm}^{-2}\ \mathrm{s}^{-1}\ \text{Å}^{-1}$. Figure 2 shows surface actinic fluxes of planets with 80% N_2, 20% CO_2, and 0.1% H_2O atmospheres with a surface pressure of 1 bar [a plausible abiotic atmosphere similar to what was likely the atmosphere of Earth 3.5 billion years ago (*13*)], within their liquid water habitable zones of a variety of stars of a variety of spectral types, compared to this limiting flux. Modern-day Earth with its 80% N_2 and 20% O_2 atmosphere is also included in this figure. Figure 3 shows the yield from a single reaction and the final concentration of pyrimidine concentration from a sequence of 10 reactions, driven by SO_3^{2-} photodetachment, as a function of surface actinic flux and temperature.

This comparison shows that the yield for the light chemistry, for each step, exceeds 50%, and therefore, early Earth meets our criterion for lying within the abiogenesis zone. The SO_3^{2-} dark chemistry is slow enough that the prebiotic inventory can be built up in regions where the surface temperature is less than ~ 20°C. The HS^- dark chemistry is more rapid, and coupled with the much smaller photodetachment cross section, the 50% yield is not achieved for the HS^- reaction even at 0°C on early Earth. The photodetachment of SO_3^{2-} is sufficiently rapid that the prebiotic inventory can be photochemically generated in a 0°C environment from the quiescent flux of a K5 dwarf ($T_{\mathrm{eff}} \approx 4400$ K).

With a clear understanding of the temperature and UV flux where the SO_3^{2-} chemistry can occur, we can now predict the planets on which this chemistry could occur. We take a catalog of all presently known potentially rocky exoplanets within the liquid water habitable zone of their host star. Using analog stellar spectra appropriate to the stellar types for the host stars in our catalog, we can show which exoplanets are primed for life and which cannot build up an appreciable prebiotic inventory. Figure 4 shows which of the liquid water habitable zone planets also lie within the abiogenesis zone. To select planets that are reasonably likely to be rocky, we impose a criterion on the planetary radius, $R_{\mathrm{p}} \leq 1.4\ R_{\oplus}$, where $R_{\oplus}$ is the radius of Earth. The question of at what radius a planet is likely rocky is difficult to answer definitively. There have been many investigations into this question [for example, (*14*–*16*)].

Stars are not quiet, and several researchers have wondered whether the frequent flaring of young ultracool dwarves may be sufficient to initiate the photochemical production of the prebiotic inventory (*10*, *11*). We explore this possibility. For our purposes, activity means variability in the wavelength range between 200 and 280 nm. This is primarily caused by flares and coronal mass ejections (CMEs). Only a series of flares of sufficient energy over a period of time determined by the dark chemistry rates will result in a 50% yield per step for the reactions along the way to the prebiotic inventory.

To account for flaring, we consider a simple model. The dark chemistry is slowest at 0°C, at which temperature high concentrations of SO_3^{2-} and HCN are consumed at a rate determined by using our measured rate constants. If a sufficient number of flares occur such that a 50% yield of the photochemical products is expected per step, then these planets meet the criterion for lying within their star's abiogenesis zone due to the stellar activity. We examine what fraction of stars cooler than K5 flare this frequently.

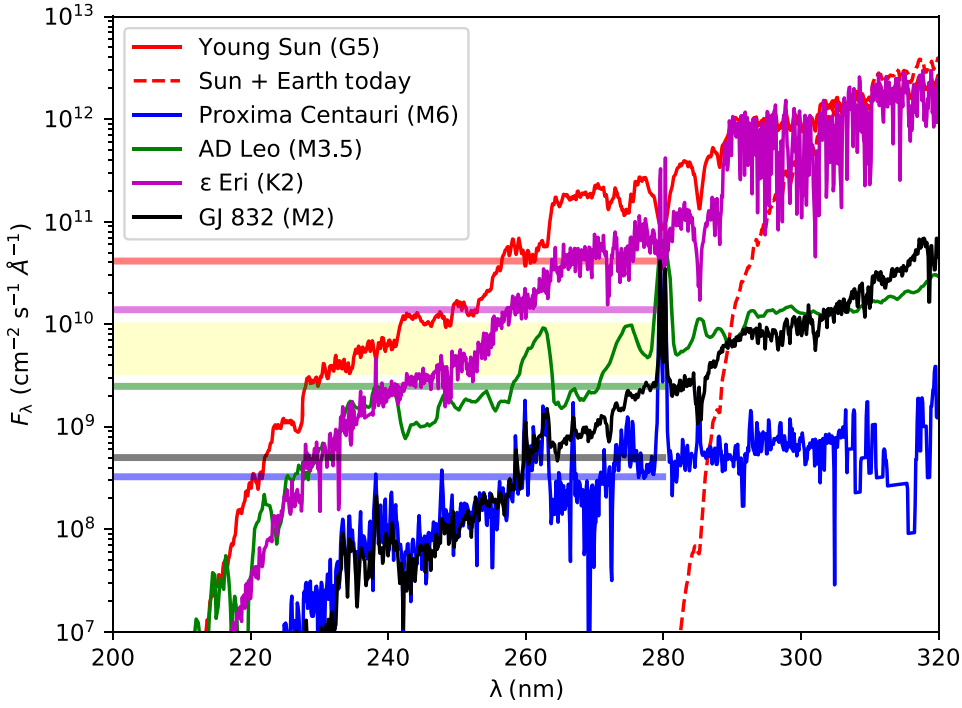

Fig. 2. Surface actinic fluxes. The surface actinic flux F_λ as a function of the wavelength λ for planets within the habitable zones of five stars (with spectral type given in the legend): early Earth in the case of the young Sun and Proxima b in the case of Proxima Centauri. For GJ832, ∈ Eri, and AD Leo, these are hypothetical planets at the innermost edge of the liquid water habitable zone to maximize the surface flux. The yellow shaded region (the width of which accounts for the errors; see Materials and Methods, especially Eqs. 27 to 30) shows the average flux needed between 200 and 280 nm for the light chemistry and dark chemistry to proceed both at the same rate at 0°C. The color-shaded horizontal lines show the average fluxes of the respective stars. The surface actinic flux of Earth today is also included. Its 200- to 280-nm flux is strongly attenuated by atmospheric ozone.

Figure 5 shows our results using present flare statistics for cool stars (*17*). We find that ~30% of stars cooler than K5, and ~20% of the early M dwarfs, are active enough for the planets they host to be within their abiogenesis zones. The statistics given by Davenport (*17*) did not concentrate on high-energy flares and is based on the Kepler sample, which does not include enough ultracool (cooler than M4) stars to provide very reliable flare statistics. Further analysis of the frequencies of energetic flares will be necessary for a more robust statistics about which exoplanets are primed for life due to the activity of their host stars. It would be especially relevant for flare rates to be determined for the stars included in Fig. 4.

Photons are also generated by the particles from the CME impinging on the upper atmosphere (*18*), but even assuming that the total kinetic energy of every >1 GeV proton from a large CME is converted into 200- to 280-nm photons, the flux would still be an order of magnitude too small to overcome the dark chemistry (see the "Coronal mass ejections" section).

DISCUSSION

Using a known reliable pathway for photochemically building up the prebiotic inventory in large yields, we show that hotter stars serve as better engines for prebiotic chemistry. Investigating the race between light and dark bisulfite chemistry, we find, based on our requirement for >50%. yields, that, even for early Earth, the prebiotic inventory would need to be built up in places where the surface temperature is below ~ 20°C. The HS^- photodetachment is too slow to allow for the prebiotic inventory to build up on early Earth. As it turns out, however, HS^- dark chemistry results in important amino acid precursors. In addition, in the absence of UV light, HS^- contributes toward a more efficient pathway to form pyrimidine nucleosides (*19*). Because UV flux of the young Sun would not have been sufficient to drive the HS^- photochemistry, the HS^- chemistry behaves as though it is taking place in the absence of UV light. With both HS^- and bisulfite present, this provides both varieties of chemistry (bisulfite light chemistry and HS^- dark chemistry) simultaneously: the best of both worlds.

Because of the efficiency of the bisulfite photochemistry, rocky planets within the liquid water habitable zones of K dwarfs can also lie within the abiogenesis zone, so long as the temperature is very close to 0°C. We applied our results to a catalog of potentially rocky exoplanets within the liquid water habitable zones of their host stars. For gas giants within the liquid water habitable zone, there is a tantalizing possibility that some of their larger moons may be primed for life (*20*).

The abiogenesis zone we define need not overlap the liquid water habitable zone. The liquid water habitable zone identifies those planets that are a sufficient distance from their host star for liquid water to exist stably over a large fraction of their surfaces. In the scenario we consider, the building blocks of life could have been accumulated very rapidly compared to geological time scales, in a local transient environment, for which liquid water could be present outside the liquid water habitable zone. The local and transient occurrences of these building blocks would almost certainly be undetectable. The liquid water habitable zone helpfully identifies where life could be sufficiently abundant to be detectable.

For main sequence stars cooler than K5 dwarfs, the quiescent stellar flux is too low for the planets within their habitable zones to also lie within their abiogenesis zones. Planets within the habitable zones of quiet ultracool dwarfs may be able to house life, but life could not presently originate as a result of photochemistry on these worlds, although it possibly could have done in the past, if these stars emitted much more strongly in the UV before they entered into the main sequence or if they

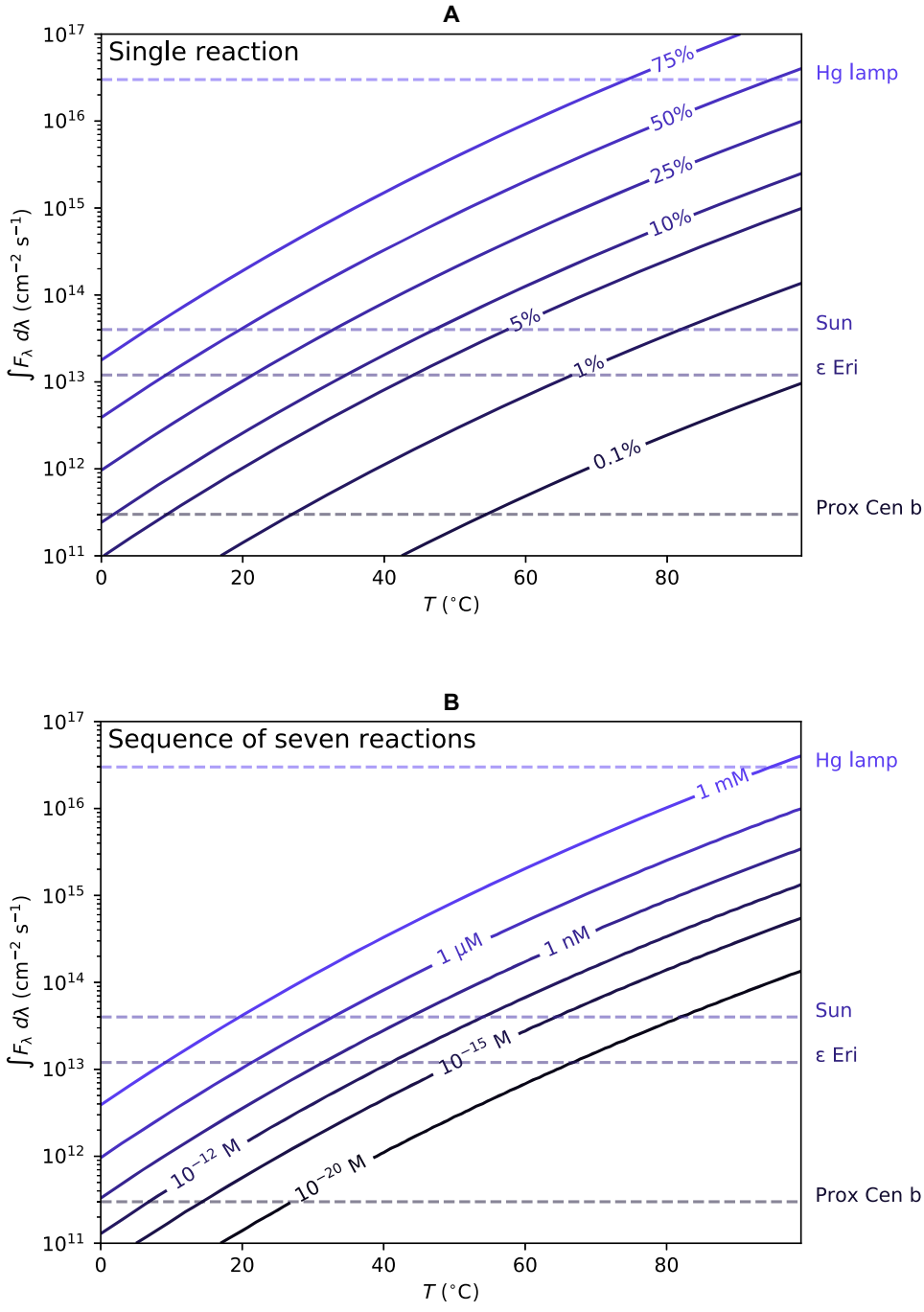

Fig. 3. Reaction yields. Contour plot of (**A**) the yield after one reaction and (**B**) the final concentration of the pyrimidines after seven consecutive reactions (three of which involve two products of a previous reaction) with initial reactants all at 1 M concentrations, as a function of temperature T (K) and the integrated surface UV flux $\int \boldsymbol{F}_\lambda\, d\lambda$ (cm^2 s^{-1}) from 200 to 280 nm, assuming that all photochemical reactions have similar cross sections and rate constants to the SO_3^{2-} reactions we measured, by multiplying the yield with itself 10 times, which accounts for the arithmetic demon for the case of 10 consecutive reactions and matches with the pseudo-equilibrium results if rate equations were applied. Comparable surface fluxes are listed on the left.

had been much more active in the past. Our results are only valid for the stars as they are now. There is a decent chance that, for the most active M dwarfs, flares could be sequentially timed during intermediate reactions along the chemical pathway to build up the prebiotic inventory.

It turns out that stellar activity is not always bad for life but may, in fact, be the only pathway to starting life on planets around ultracool stars. If the activity of an ultracool dwarf decreases as it ages, there might be sufficient 200- to 280-nm light from flares to initiate life on these planets soon after the star's formation; as the star gets older, the 200- to 280-nm light could decrease to a low enough level so that the resulting RNA will not be damaged as frequently, although flares may still pose a problem for the stability of RNA strands.

There are other theories about how the prebiotic inventory could be generated, either on the surface of the planet (*21*, *22*) or on interstellar

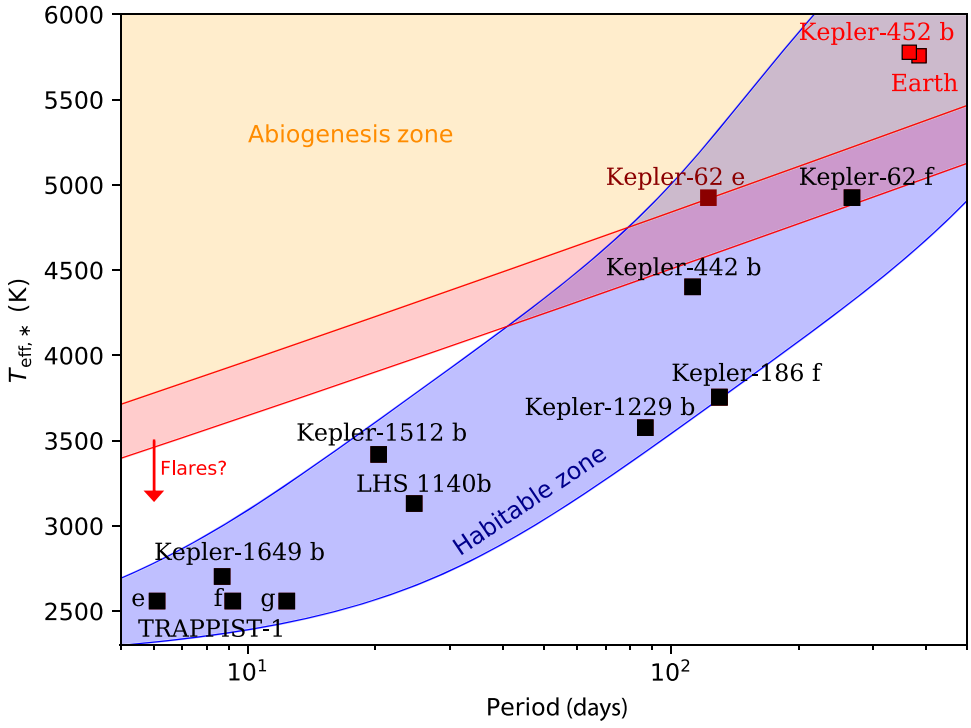

Fig. 4. Abiogenesis zone. A period-effective temperature diagram of confirmed exoplanets within the liquid water habitable zone (and Earth), taken from a catalog (*1*, *42*, *43*), along with the TRAPPIST-1 planets (*3*) and LHS 1140b (*4*). The "abiogenesis zone" indicates where the stellar UV flux is large enough to result in a 50% yield of the photochemical product. The red region shows the propagated experimental error. The liquid water habitable zone [from (*44*, *45*)] is also shown.

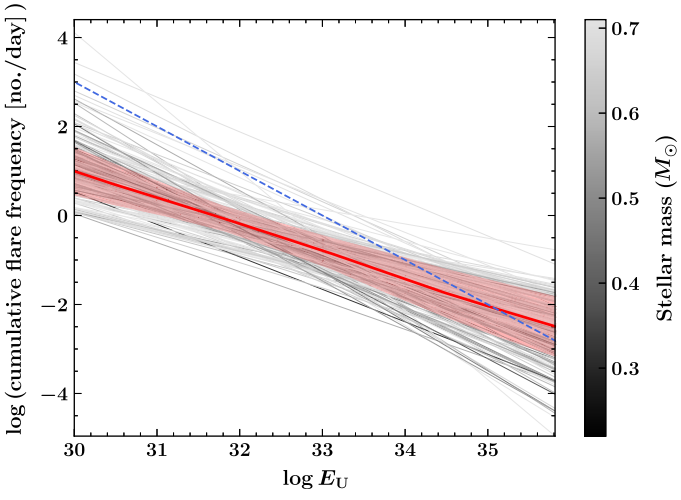

Fig. 5. Flare frequencies. The power-law fits for the cumulative flare frequencies above a particular U-band energy, log (E_{U}/1 erg), given for a variety of Kepler stars from Davenport (*17*). The grayscale indicates stellar mass, the red line indicates the average stellar flare frequency for stars later than K5, and the blue dashed line indicates the lower limit of flaring needed: If the star's power-law flare frequency intersects the dotted blue line, then the star is active enough for its planets to be considered within the abiogenesis zone. Flares with $E_{\mathrm{U}} > 10^{35}$ are often extrapolations of flare frequencies beyond what has been observed, and flare frequencies may not follow the same power-law at these high energies (*17*).

ices (*23*). These other theories may provide plausible pathways to form a variety of amino acids, or some of the nucleobases, and so may help provide some of the building blocks of life, if somehow the relevant species can be selectively concentrated, but none of these theories has offered prebiotically plausible chemical pathways to high yields of a range of nucleotides, amino acids, and lipid precursors from prebiotically plausible starting conditions, which remains a necessary first step for the origin of life. For hypothetical alternative theories, if there is a clear link between their chemical pathways and observable physical conditions of the planet or system, then a similar analysis can be carried out and abiogenesis zones can be identified for them.

What do our results say about looking for biosignatures on rocky planets around ultracool dwarfs? This is an important consideration, given that ultracool dwarfs are likely the only possible candidates for this search within the next decade or so. Present flare statistics for cool stars suggest that as many as 20% of M dwarfs may flare often enough to drive the prebiotic photochemistry on rocky planets within their habitable zones, assuming that the atmospheres of these planets can survive this extreme activity. What is most relevant for biosignature detection would be the flare rates for M dwarfs early in their evolution, because we will want to search for biosignatures on planets where life has existed long enough to change the planet's surface and atmosphere in detectable ways. Note that the liquid water habitable zones of M dwarfs evolve inward as they age (*24*). If atmospheres are observed for a large fraction of rocky planets around active ultracool stars, then it may well be the case that life is more likely to have originated in systems with the most active stars, all else being equal.

The search for biosignatures on planets around quiet M dwarfs remains worthwhile, in some senses even more now than before our investigation. If definitive biosignatures were discovered within the atmospheres of multiple rocky planets around quiet ultracool dwarfs, at the very least, then such findings would suggest that the mechanism by which Earth-like life could originate is not universal.

MATERIALS AND METHODS

Experimental design

To determine the spectral irradiance of the lamps used in the photochemistry experiments presented here, we used a calibrated Ocean Optics FLAME-S UV-Vis spectrometer with a UV cosine-corrected irradiance probe (connected with a 2-m length of a 600-μm UV fiber). The probe collects radiant light with a Lambertian 180° field of view. The spectrometer was calibrated using the Ocean Optics DH-3-CAL, DH-3-CAL-EXT Calibrated Deuterium, and Halogen light source, valid from 200 to 700 nm. The measurements were conducted within a Rayonet UV reactor, which is set up with 16 Hg lamps. A diagram illustrating the general experimental setup is shown in fig. S1. For this study, we only consider the flux in the emission line at 254 nm, which contributes to approximately 90% of the total spectral irradiance over the 200- to 400-nm wavelength region.

The total UV flux received by the sample was calculated by first taking a measurement with the spectrometer at the approximate center of the quartz cuvette, 1 cm from the nearest lamp. Every lamp/cuvette position was measured in the same way to verify that the irradiance from each lamp is approximately equal. Given that the spectrometer probe only has a 180° field of view and that the cuvette effectively sees all the lamps, the irradiance received by one cuvette was then calculated by measuring the flux received by the cuvette by the nearest lamp only (with the other lamps switched off) and then using this measurement to calculate the contribution of all the other lamps based on their distance away from the center of the cuvette.

The measured spectrum over the wavelength range from 200 to 400 nm, with the sample flux calculated as previously described, is shown in fig. S2. The best-fit Gaussian profile for the emission line at 254 nm is shown by the dotted line in fig. S2 and is described by Eq. 5. The total UV flux received by a sample is then the area under this curve multiplied by the total surface area of the cuvette and the duration time the sample is illuminated for

$$F_{\lambda,\mathrm{lamp}} = \frac{F_0 \Delta\lambda}{\sigma\sqrt{2\pi}} e^{-(\lambda-\lambda_0)^2/(2\sigma^2)} \tag{5}$$

where $F_0 = 2.54 \times 10^{15}$ cm^{-2} s^{-1} Å^{-1}, $\lambda_0 = 254$ nm, $\sigma = 0.6$ nm, and $\Delta\lambda = 1$ nm.

Model

To determine the UV spectral irradiance on the surface of an exoplanet, we have to start with the irradiance of the star from space. To do so, we took the MUSCLES version 2.1 spectra of Proxima Cen, GJ832, and ∈ Eri (*25*–*27*). For early Earth, we took a solar analog spectrum of κ1 Ceti (*28*). For AD Leo, we used the spectrum from Segura *et al.* (*29*) (incomplete for the FUV). In all cases, these spectra are taken from Earth and are in units of erg cm^{-2} s^{-1} Å^{-1}, which flux we will call $S_{\lambda,\oplus}$. From here, we need to get the flux at the very top of our exoplanet's atmosphere $S_{\lambda,p}$, in units of photons cm^{-2} s^{-1} Å^{-1}, and to do so, we take

$$S_{\lambda,p} = \frac{hc}{\lambda}\frac{a^2}{d^2} S_{\lambda,\oplus} \tag{6}$$

where d is the distance from the star to the observer, and a is the semimajor axis of the hypothetical planet, always chosen so that the bolometric flux from the star is identical to the bolometric flux from the Sun, following earlier work (*30*). Here, h is Planck's constant, c is the speed of light, and λ (nm) is the wavelength of the light. $S_{\lambda,p}$ is shown in fig. S3.

We took these spectra and applied them as the top boundary condition to the ARGO photochemistry/diffusion code (*31*). This code solves the set of photochemical kinetics equations for a moving parcel of atmospheric gas

$$\frac{\partial n_i}{\partial t} = P_i - L_i - \frac{\partial \Phi_i}{\partial z} \tag{7}$$

for an atmosphere of bulk composition 80% N_2 and 20% CO_2 and other species from the bottom of the atmosphere in trace amounts. This is similar to the presumed atmosphere of early Earth (*13*). Given that volatile acquisition is unsolved for our own solar system and that the secondary atmosphere is determined primarily by the outgassing pressure and C/O ratio, CO_2 is expected to be a dominant component of the atmosphere of a rocky planet of approximately Earth mass and with a crustal and upper mantle C/O ratio of ≲0.8 (*32*, *33*). Why Earth has its present quantity of atmospheric nitrogen is a mystery, and at present, we have no alternative recourse but to assume similar amounts of N_2 in the atmospheres of rocky exoplanets. Because N_2 does not absorb in UV between 200 and 280 nm (*8*), its presence or absence by itself should not significantly affect these results. Here, n_i (cm^{-3}) is the number density of species i, where $i = 1,\ldots, I_s$, I_s being the total number of species. P_i(cm^{-3} s^{-1}) and L_i (cm^{-3} s^{-1}) represent the production and loss rates, which are determined by using the STAND chemical network (*31*). The quantity Φ_i is the flux of the species i into and out of the parcel when it is at height z. As described in (*31*), the parcel is used to give a chemical profile of the atmosphere, and UV photo-transport is calculated to determine the efficiency of the photochemistry at each parcel height. At the very end, the surface actinic flux was determined by taking $S_{\lambda,p} = F_\lambda(z_{\mathrm{top}})$, where z_{top} (cm) is the height of the top of the atmosphere, above which the UV light in consideration is virtually unattenuated. The surface atmospheric flux is then

$$F_\lambda(z=0) = S_{\lambda,p} e^{-\tau(\lambda,z=0)/\mu_0} + F_{\mathrm{d}} \tag{8}$$

where τ is the optical depth determined using the chemical profile and is unitless, F_{d} is the diffusive actinic flux determined using the δ-Eddington two-stream method (*34*), and μ_0 is the cosine of the stellar zenith angle, which we set = 1 to achieve the maximum surface flux, the best-case scenario for our light chemistry. The surface UV actinic fluxes for the hypothetical or real habitable zone planets around the young Sun, Proxima Cen, GJ832, and ∈ Eri are shown in the main paper.

To compare our model to data, we used the Ocean Optics spectrometer and measured the Sun outside the Laboratory of Molecular Biology in Cambridge on 24 February 2017 at 1500. We used the National Oceanic and Atmospheric Administration Solar Calculator (www.esrl.noaa.gov/gmd/grad/solcalc/azel.html) to determine the cosine of the zenith angle and applied our model with an 80% N_2 and 20% O_2 atmosphere, with some trace constituents. The comparison between our model and the data is given in fig. S4.

Rate constants

In this section, we consider the kinetics for the reactions discussed in the Supplementary Materials. The kinetics two "dark" reactions we consider (bimolecular reactions in the absence of 254 nm of light)

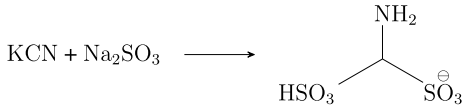

(9)

(10)

follow the rate equation mediated by the rate constant k_r (liter mol^{-1} s^{-1})

$$\frac{dx}{dt} = k(c_0 - x)^2 \tag{11}$$

for stoichiometrically balanced initial concentrations of reactants [c_0 (M)], where x is the concentration of the adduct. The solution to this equation, considering the boundary condition where $x(0) = 0$, is

$$x(t) = c_0 - \frac{1}{\frac{1}{c_0} + k_r t} \tag{12}$$

We used this solution, along with the nuclear magnetic resonance (NMR) measurements of the products discussed in section S2, to solve for k. The NMR measurements were taken for mixtures of KCN + Na_2SO_3, as well as NaHS· xH_2O + C_2H_3NO, at different temperatures, but with the same initial c_0. We refer to the KCN + Na_2SO_3 reaction by the reaction that takes place from this starting material in water: SO_3^{2-} + HCN and NaHS· xH_2O + C_2H_3NO by HS^- + C_2H_3NO. By measuring either the product or, where possible, both product and reactant, we determined the concentration of the adduct, x, and used this to solve for kt. For some temperatures, we made multiple measurements of k to estimate the variance. The errors in these measurements are dominated by errors in weighing the reactants and, in the case of HS^-, the loss of the bound H_2O and the escape of the reactant in the form of H_2S.

The resulting concentrations, times, and rate coefficients are shown for each measurement in tables S1 and S2. Arrhenius plots for both bimolecular reactions can be produced (fig. S5). These were fit using the SciPy routine, assuming the standard Arrhenius form for the rate coefficient, in this case

$$\log k_r = \log\left(\frac{\alpha}{1\ \text{mol}^{-1}\ \text{liter}\ \text{s}^{-1}}\right) - \frac{E_a}{T} \tag{13}$$

where α is the prefactor, the rate coefficient for the reaction at a hypothetical infinite temperature; E_a (K) is the activation energy; and T (K) is the temperature of the solution. For the two reactions, we achieve the following results

$$\log \alpha\left(SO_3^{2-} + \text{HCN}\right) = 18.7 \pm 0.32\ \text{mol}^{-1}\ \text{liter}\ \text{s}^{-1} \tag{14}$$

$$E_a\left(SO_3^{2-} + \text{HCN}\right) = 9490 \pm 106\ \text{K} \tag{15}$$

$$\log \alpha(HS^- + C_2H_3NO) = 12.2 \pm 0.3\ \text{mol}^{-1}\ \text{liter}\ \text{s}^{-1} \tag{16}$$

$$E_a(HS^- + C_2H_3NO) = 7480 \pm 130\ \text{K} \tag{17}$$

which are placed in more natural units within the main text.

For the light chemistry (photodetachment reactions under 254-nm light, as well as the bimolecular reactions), we consider the reactions

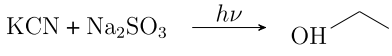

(18)

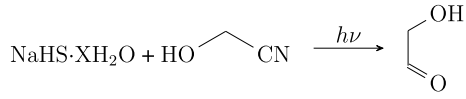

(19)

It should be noted that, in the case of KCN + Na_2SO_3, many of the photochemical products are intermediates toward glycolonitrile, such as aminomethanesulfonate and azanediyldimethanesulfonate, which will proceed under the conditions we consider (pH 7) almost completely to glycolonitrile via reactions that proceed without the UV light (*6*). As explained above, the abundance of these intermediates is included and treated here as though the intermediates were glycolonitrile.

The rate coefficients for these reactions are determined in terms of the consumption of the reactant, y (M), mediated by both the photodetachment rate k_λ (s^{-1}) and the bimolecular reaction k_r (liter mol^{-1} s^{-1}), same as above

$$\frac{dy}{dt} = -k_r y^2 - k_\lambda y \tag{20}$$

which can be integrated directly to achieve

$$-k_\lambda t = \log\left(\frac{y}{y + \frac{k_\lambda}{k_r}}\right) + C \tag{21}$$

where C is the constant of integration. This is left as the following equation, with C solved for the boundary condition $y(0) = c_0$

$$\frac{y}{y + \frac{k_\lambda}{k_r}} = \left(\frac{c_0}{c_0 + \frac{k_\lambda}{k_r}}\right) e^{-k_\lambda t} \tag{22}$$

This solution is used to numerically solve for k_λ under different fluxes for the SO_3^{2-} chemistry by placing the mixture within the reactor when all the lamps are on, by having half the lights on and placing the mixture near one of the lights that is on, and by having half the lights on and placing the mixture near one of the lights that is off. The actinic flux for these three cases was calculated in the "Experimental design" section. When k_λ is solved, we made the assumption, which has weak empirical support (*9*, *35*), that the reaction cross section for photodetachment, σ_λ (cm^2), is constant over the range from 200 to 280 nm.

Given the actinic flux, F_λ (photons cm^{-2} s^{-1} Å^{-1}), and the equation for the photochemical rate constant

$$k_\lambda = \int_{200\ \mathrm{nm}}^{280\ \mathrm{nm}} F_\lambda \sigma_\lambda d\lambda \quad (23)$$

and because we are assuming that σ_λ is constant over the range of λ, it comes out in front of the integral, and the integral of F_λ is simply the prefactor for the Gaussian fit to the peak 254 nm lamp flux (see the "Experimental design" section). In this way, we took the product of the irradiation, z (M), and the product of the dark chemistry occurring alongside the light chemistry, x (M), and set $y = c_0 - x - z$. We then numerically solved for $k_v t$ from the above solution, divided by the time under which the mixture has been irradiated, and divided again by $\int F_\lambda\, d\lambda$ to determine that

$$\sigma_\lambda\left(SO_3^{2-} + HCN\right) = (1.5 \pm 0.3) \times 10^{-20}\ \mathrm{cm}^2 \quad (24)$$

We were unable to perform the same analysis for HS^-, because HS^- is not as soluble and escapes the mixture and oxidizes, which would require us to incorporate other loss terms in our kinetics equation. Instead, we have taken a different approach, as discussed above, and saturated our mixture with HS^- compared to the glycolonitrile. This modifies the rate equation to

$$\frac{dy}{dt} = -k_r y_0 y - k_\lambda y \quad (25)$$

where y in this case is the concentration of the glycolonitrile, and y_0 is the HS^-, which is effectively constant compared to the glycolonitrile. This is a linear differential equation with the solution

$$y(t) = c_0 e^{-(k_r y_0 + k_\lambda)t} \quad (26)$$

We used the dark chemistry values for k_r, used our initial concentration of HS^- for y_0 and the initial concentration of glycolonitrile for c_0, and solved for k_λ. Then, with the same assumption of the constant photochemical cross section, we applied k_λ to Eq. 23 and found

$$\sigma_\lambda(HS^- + C_2H_3NO) = (2.0 \pm 0.4) \times 10^{-23}\ \mathrm{cm}^2 \quad (27)$$

The values of σ_λ from Eqs. 24 and 27 are the same value to within the error bars.

To quantify the competition between "light" and dark chemistry, we compared the half-lives of the two reactions. In the light, this is simply

$$t_{\mathrm{light}} = \frac{\log 2}{\int_{200\ \mathrm{nm}}^{280\ \mathrm{nm}} F_\lambda \sigma_\lambda d\lambda} \quad (28)$$

$$= \frac{\log 2}{\sigma_\lambda \overline{F}_\lambda \Delta\lambda} \quad (29)$$

where $\overline{F}_\lambda$ (cm^{-2} s^{-1} Å^{-1}) is the average actinic flux at the surface between 200 and 280 nm, and $\Delta\lambda$ = 80 nm is the relevant wavelength range.

The half-life for the dark reaction is

$$t_{\mathrm{dark}} = \frac{1}{c_0 k_r} \quad (30)$$

We took the most favorable temperature for the reactions: a surface temperature of 0°C. We assumed a high initial concentration of reactants, c_0 = 1 M. Although this makes the dark reaction fast, decreasing this value significantly will frustrate subsequent bimolecular reactions needed for the pyrimidine synthesis. The effect of decreasing the concentration has a linear effect on the rate for the reaction in the dark but has a quadratic effect on the rates of these subsequent bimolecular reactions.

We set the $t_{\mathrm{light}} = t_{\mathrm{dark}}$ and solve for $\overline{F}_\lambda$

$$\overline{F}_\lambda = \frac{c_0 k_r \log 2}{\sigma_\lambda \Delta\lambda} \quad (31)$$

Propagating the errors through this equation gives us

$$\Delta\bar{F}_\lambda = \frac{c_0 \log 2}{\Delta\lambda \sigma_\lambda} \sqrt{(\Delta k_r)^2 + \frac{k_r^2}{\sigma_\lambda^2}(\Delta\sigma_\lambda)^2} \quad (32)$$

where Δk_r is the error in the bimolecular rate constant, from Eqs. 14 to 17, and $\Delta\sigma_\lambda$ is the error in the photochemical cross section, from Eqs. 24 and 27. For the light chemistry to compete with the dark chemistry at 0°C, we found that, for SO_3^{2-}

$$F_\lambda = (6.8 \pm 3.6) \times 10^9\ \mathrm{cm}^{-2}\ \mathrm{s}^{-1}\ \text{Å}^{-1} \quad (33)$$

and for HS^-

$$F_\lambda = (1.6 \pm 0.4) \times 10^{12}\ \mathrm{cm}^{-2}\ \mathrm{s}^{-1}\ \text{Å}^{-1} \quad (34)$$

integrated over 200 to 280 nm. For SO_3^{2-}, this is the rough equivalent of the integrated quiescent flux of a K5 dwarf ($T_{\mathrm{eff}} \approx 4400$ K).

Flare rates

When we model the flares, we consider the spectrum of the 12 April 1985 AD Leo flare as our sole template (*36*). This flare had an energy in the U band of $E_U = 10^{34}$ erg. We then changed the spectrum as a function of time following the spectral evolution given by (*37*). This suffices to describe the time evolution of the UV flux for a 10^{34} erg flare, which we assume here can be applied in the same way to all stars. We scale the peak flux and duration using flare statistics from Hawley *et al.* [(*38*), their figure 10]. We then passed it through the atmosphere as described (see the "Model" section). This is how we produce fig. S6. Our treatment of the flares, however, can rest more generally on the flare statistics, without worrying as much about the specifics of the AD Leo flare.

The total number of photons necessary within the lifetime of the reactant for a 50% yield of the photochemical product is

$$n_{\gamma,r} = \frac{1}{\sigma_\lambda \Delta\lambda} = 8.3 \times 10^{16}\ \mathrm{cm}^{-2}\ \mathrm{\AA}^{-1} \quad (35)$$

using the value of σ_λ from Eq. 24.

We note that the spectrum of the AD Leo flare is relatively flat at wavelengths shorter than the U band, and so the total number of photons $\mathrm{cm}^{-2}\ \mathrm{\AA}^{-1}$ will be the same between 200 and 280 nm as it is within the U band. Hence, we can estimate the total fluence (the total number of photons deposited during the length of the flare) at the planet's surface for photons between 200 and 280 nm to be linearly proportional to the flare energy in the U band, or

$$n_{\gamma,f} = 2.4 \times 10^{16}\ \mathrm{cm}^{-2}\ \mathrm{\AA}^{-1} \left(\frac{E_\mathrm{U}}{10^{34}\ \mathrm{erg}}\right) \quad (36)$$

This equation relies on correlations between the fluence of the flare and its energy in the U band. This can vary considerably, leading to large errors. For the reaction to exceed 50% conversion, $n_{\gamma,f} \geq n_{\gamma,r}$.

Flare frequencies follow a power-law distribution (*38*, *39*) such that

$$\log \nu = \log \alpha + \beta \log E_\mathrm{U} \quad (37)$$

where ν (day^{-1}) is the cumulative flare frequency for all flares of U-band energy greater than E_U, and α and β are coefficients for the power-law fit. This equation gives us our constraint on which power laws are necessary for building up the prebiotic inventory. We solved for ν after applying Eqs. 35 and 36, to find

$$\nu = \frac{8 \times 10^{27}\ \mathrm{erg/s}}{E_\mathrm{U}} \quad (38)$$

For the power laws published by Hilton (*39*), which come from targeted ground-based observations of ~25 stars, only those for the very active M3 to M5 dwarfs qualify.

The Kepler mission, while not specifically targeting M dwarfs, still observed many of these low-mass stars that fell within its field of view. Multiple studies have analyzed flares in Kepler data (*17*, *38*, *40*). A homogeneous search for stellar flares was performed by Davenport (*17*) using all available Kepler light curves. Kepler data span 3.5 years, which provide a suitable baseline from which to estimate flare rates. Flares were detected on ~2% of all Kepler stars (~4000 in total), and flare frequency distributions (FFDs) were computed.

We took the Davenport FFDs and calculated the percentage of those FFDs that would produce enough flares to satisfy Eq. 38. To do this, we (i) converted energy in the Kepler band to the U band following the relation presented in (*38*) (that is, $E_\mathrm{U} = 0.65 E_{K_\mathrm{p}}$), (ii) removed eclipsing binaries through cross-matching with the Kepler Eclipsing Binary Catalogue V3 (*41*), and (iii) required a system to show a cumulative flare frequency of at least 1 day^{-1} at $E_\mathrm{U} \geq 1 \times 10^{30}$ erg, which removes nonactive stars and hence lowers the chances of extrapolating the FFDs.

Figure 5 shows the FFDs for all stars passing our selection criteria. We evaluated the stars whose power-law flare rates cross the power law of Eq. 38 as potentially hosting planets within their abiogenesis zones. We split the flare stars into different mass bins and report the percentages of sufficiently active stars in table S3. We found that the highest flare rates are for stars between = 0.6 to 0.7 $M_\odot$.

Although we made our best efforts to remove eclipsing binaries, for which it is more difficult to identify flares, for which flaring rates might be very different, and for which the question of habitability is more controversial, we have not been able to remove all binaries. Namely, we have not been able to remove the non-eclipsing binaries from our sample. Furthermore, the statistics from Davenport's sample often require extrapolations, sometimes extreme, from the energies at which the flares were observed to the higher-energy flares. Extrapolating this much off of a power law is always fraught with risk, especially when Davenport has pointed out that it is common to find breaks in the power laws for flare rates [figure 6 of (*17*)]. Extrapolating to low energies is also unreliable, because Davenport's methods for detecting flares may not be sensitive to flares below a certain energy.

However, because in every example given, the power law breaks steeper, our statistics will provide at the very least a reliable upper limit for the number of stars earlier than M4, for which flares are both energetic enough and frequent enough to produce the prebiotic inventory (see table S3). We note that previous studies found that flares are more frequent on mid-M dwarfs (M3 to M5) than on earlier-M dwarfs (M0 to M2) but typically have lower energies. Because of all these uncertainties and contradictory findings, it will be important to reanalyze flare rates from data and possibly new observations, concentrating on very energetic flares, with energies above 10^{34} erg. It will be especially useful to perform these statistics for those stars from the Kane catalog (*1*) and host stars for rocky planets potentially within their habitable zones.

Coronal mass ejections

To estimate the effect of energetic particles from a CME on the UV surface flux, we considered only those particles that impinge on the upper atmosphere effectively, without being deflected by the planetary magnetic field, and that will produce particle showers upon impact with the atmosphere. This restricts us mostly to CME protons of energy greater than 1 GeV. For our analysis, we used the same energy distribution of CME protons as (*18*), or

$$j(E) = 1.26 \times 10^6\ \mathrm{protons\ cm}^{-2}\ \mathrm{GeV}^{-1} \left(\frac{E}{1\ \mathrm{GeV}}\right)^{-2.15} \quad (39)$$

where E (GeV) is the proton energy. We consider that a CME of this strength impinges on the atmosphere every 5.8 min (τ_CME = 350 s), based on the CME event rates estimated by (*18*). We make the assumption that the energy of every CME proton is converted entirely into photons of wavelength λ_0 = 280 nm. This assumption is unphysical, but it provides a hard upper limit to the impact of the CME particles on the UV photochemistry. In this case, the number of photons produced by a cosmic ray of energy E is

$$N_\gamma = \frac{E\lambda_0}{hc} \quad (40)$$

where h is Planck's constant and c is the speed of light. The photochemical rate constant in this case will be the total number of 280-nm

photons times the cross section at 280 nm or, for SO_3^{2-}, where $\sigma_\lambda = 1.5 \times 10^{-21}$ cm^2

$$k_{\lambda,\mathrm{CME}} = \frac{\lambda_0 \sigma_\lambda}{hc\tau_{\mathrm{CME}}} \int_{1\ \mathrm{GeV}}^{\infty} Ej(E)dE \quad (41)$$

The solution is that $k_{\lambda,\mathrm{CME}} = 8.1 \times 10^{-9}$ s, giving a half-life for the light chemistry due to CMEs of about 2.7 years. This is too slow to produce the prebiotic inventory.

SUPPLEMENTARY MATERIALS

Supplementary material for this article is available at http://advances.sciencemag.org/cgi/content/full/4/8/eaar3302/DC1

Fig. S1. The UV reactor.
Fig. S2. Reactor emission plot of the measured (solid line) emission from the Hg lamps over the 200- to 400-nm spectral range.
Fig. S3. Stellar spectra.
Fig. S4. Surface spectral irradiance at Cambridge.
Fig. S5. Arrhenius plots.
Fig. S6. Flare spectra.
Table S1. HCN + SO_3^{2-}.
Table S2. Glycolonitrile + HS^-.
Table S3. Percentages of stars in different spectral type ranges that meet the criterion for activity given by Eq. 38 (defined here as "Active" stars).
Section S1. General procedures for reactions of KCN with Na_2SO_3 in the dark.
Section S2. General procedures for reactions of KCN with Na_2SO_3 under UV light.
Section S3. General procedures for reactions of glycolonitrile with NaHS in the dark.
Section S4. General procedures for reactions of glycolonitrile with NaHS under UV light.
References (*46*–*48*)

REFERENCES AND NOTES

1. S. R. Kane, M. L. Hill, J. F. Kasting, R. K. Kopparapu, E. V. Quintana, T. Barclay, N. M. Batalha, W. J. Borucki, D. R. Ciardi, N. Haghighipour, N. R. Hinkel, L. Kaltenegger, F. Selsis, G. Torres, A catalog of Kepler habitable zone exoplanet candidates. *Astrophys. J.* **830**, 1 (2016).
2. G. Anglada-Escudé, P. J. Amado, J. Barnes, Z. M. Berdiñas, R. P. Butler, G. A. L. Coleman, I. de La Cueva, S. Dreizler, M. Endl, B. Giesers, S. V. Jeffers, J. S. Jenkins, H. R. A. Jones, M. Kiraga, M. Kürster, M. J. López-González, C. J. Marvin, N. Morales, J. Morin, R. P. Nelson, J. L. Ortiz, A. Ofir, S.-J. Paardekooper, A. Reiners, E. Rodríguez, C. Rodríguez-López, L. F. Sarmiento, J. P. Strachan, Y. Tsapras, M. Tuomi, M. Zechmeister, A terrestrial planet candidate in a temperate orbit around Proxima Centauri. *Nature* **536**, 437–440 (2016).
3. M. Gillon, A. H. M. J. Triaud, B.-O. Demory, E. Jehin, E. Agol, K. M. Deck, S. M. Lederer, J. de Wit, A. Burdanov, J. G. Ingalls, E. Bolmont, J. Leconte, S. N. Raymond, F. Selsis, M. Turbet, K. Barkaoui, A. Burgasser, M. R. Burleigh, S. J. Carey, A. Chaushev, C. M. Copperwheat, L. Delrez, C. S. Fernandes, D. L. Holdsworth, E. J. Kotze, V. Van Grootel, Y. Almleaky, Z. Benkhaldoun, P. Magain, D. Queloz, Seven temperate terrestrial planets around the nearby ultracool dwarf star TRAPPIST-1. *Nature* **542**, 456–460 (2017).
4. J. A. Dittmann, J. M. Irwin, D. Charbonneau, X. Bonfils, N. Astudillo-Defru, R. D. Haywood, Z. K. Berta-Thompson, E. R. Newton, J. E. Rodriguez, J. G. Winters, T.-G. Tan, J.-M. Almenara, F. Bouchy, X. Delfosse, T. Forveille, C. Lovis, F. Murgas, F. Pepe, N. C. Santos, S. Udry, A. Wünsche, G. A. Esquerdo, D. W. Latham, C. D. Dressing, A temperate rocky super–Earth transiting a nearby cool star. *Nature* **544**, 333–336 (2017).
5. B. H. Patel, C. Percivalle, D. J. Ritson, C. D. Duffy, J. D. Sutherland, Common origins of RNA, protein and lipid precursors in a cyanosulfidic protometabolism. *Nat. Chem.* **7**, 301–307 (2015).
6. J. Xu, D. J. Ritson, S. Ranjan, Z. R. Todd, D. D. Sasselov, J. D. Sutherland, Photochemical reductive homologation of hydrogen cyanide using sulfite and ferrocyanide. *Chem. Commun.* **54**, 5566–5569 (2018).
7. J. D. Sutherland, Opinion: Studies on the origin of life—The end of the beginning. *Nat. Rev. Chem.* **1**, 0012 (2017).
8. S. Ranjan, D. D. Sasselov, Influence of the UV environment on the synthesis of prebiotic molecules. *Astrobiology* **16**, 68–88 (2016).
9. Z. R. Todd, A. C. Fahrenbach, C. J. Magnani, S. Ranjan, A. Björkbom, J. W. Szostak, D. D. Sasselov, Solvated-electron production using cyanocuprates is compatible with the UV-environment on a Hadean–Archaean Earth. *Chem. Commun.* **54**, 1121–1124 (2018).
10. S. Rugheimer, A. Segura, L. Kaltenegger, D. D. Sasselov, UV surface environment of Earth-like planets orbiting FGKM stars through geological evolution. *Astrophys. J.* **806**, 137 (2015).
11. S. Ranjan, R. Wordsworth, D. D. Sasselov, The surface UV environment on planets orbiting M-dwarfs: Implications for prebiotic chemistry and the need for experimental follow-up. *Astrophys. J.* **843**, 110 (2017).
12. G. A. Crispino, P. T. Ho, K. B. Sharpless, Selective perhydroxylation of squalene: Taming the arithmetic demon. *Science* **259**, 64–66 (1993).
13. J. F. Kasting, Earth's early atmosphere. *Science* **259**, 920–926 (1993).
14. L. A. Rogers, Most 1.6 Earth-radius planets are not rocky. *Astrophys. J.* **801**, 41 (2015).
15. A. Wolfgang, E. Lopez, How rocky are they? The composition distribution of *Kepler*'s sub-Neptune planet candidates within 0.15 AU. *Astrophys. J.* **806**, 183 (2015).
16. J. Chen, D. Kipping, Forecasted masses for seven thousand KOIs. *Mon. Not. R. Astron. Soc.* **473**, 2753 (2017).
17. J. R. A. Davenport, The *Kepler* catalog of stellar flares. *Astrophys. J.* **829**, 23 (2016).
18. V. S. Airapetian, A. Glocer, G. Gronoff, E. Hébrard, W. Danchi, Prebiotic chemistry and atmospheric warming of early Earth by an active young Sun. *Nat. Geosci.* **9**, 452–455 (2016).
19. J. Xu, M. Tsanakopoulou, C. J. Magnani, R. Szabla, J. E. Šponer, J. Šponer, R. W. Góra, J. D. Sutherland, A prebiotically plausible synthesis of pyrimidine β-ribonucleosides and their phosphate derivatives involving photoanomerization. *Nat. Chem.* **9**, 303–309 (2016).
20. D. Forgan, D. Kipping, Dynamical effects on the habitable zone for Earth-like exomoons. *Mon. Not. R. Astron. Soc.* **432**, 2994–3004 (2013).
21. H. J. Cleaves, J. H. Chalmers, A. Lazcano, S. L. Miller, J. L. Bada, A reassessment of prebiotic organic synthesis in neutral planetary atmospheres. *Orig. Life Evol. Biosph.* **38**, 105–115 (2008).
22. K. Ruiz-Mirazo, C. Briones, A. de la Escosura, Prebiotic systems chemistry: New perspectives for the origins of life. *Chem. Rev.* **114**, 285–366 (2014).
23. M. P. Bernstein, J. P. Dworkin, S. A. Sandford, G. W. Cooper, L. J. Allamandola, Racemic amino acids from the ultraviolet photolysis of interstellar ice analogues. *Nature* **416**, 401–403 (2002).
24. A. J. Rushby, M. W. Claire, H. Osborn, A. J. Watson, Habitable zone lifetimes of exoplanets around main sequence stars. *Astrobiology* **13**, 833–849 (2013).
25. K. France, R. O. P. Loyd, A. Youngblood, A. Brown, P. C. Schneider, S. L. Hawley, C. S. Froning, J. L. Linsky, A. Roberge, A. P. Buccino, J. R. A. Davenport, J. M. Fontenla, L. Kaltenegger, A. F. Kowalski, P. J. D. Mauas, Y. Miguel, S. Redfield, S. Rugheimer, F. Tian, M. C. Vieytes, L. M. Walkowicz, K. L. Weisenburger, The MUSCLES Treasury Survey. I. Motivation and overview. *Astrophys. J.* **820**, 89 (2016).
26. A. Youngblood, K. France, R. O. P. Loyd, J. L. Linsky, S. Redfield, P. C. Schneider, B. E. Wood, A. Brown, C. Froning, Y. Miguel, S. Rugheimer, L. Walkowicz, The MUSCLES Treasury Survey. II. Intrinsic LYα and extreme ultraviolet spectra of K and M dwarfs with exoplanets*. *Astrophys. J.* **824**, 101 (2016).
27. R. O. P. Loyd, K. France, A. Youngblood, C. Schneider, A. Brown, R. Hu, J. Linsky, C. S. Froning, S. Redfield, S. Rugheimer, F. Tian, The MUSCLES Treasury Survey. III. X-ray to infrared spectra of 11 M and K stars hosting planets. *Astrophys. J.* **824**, 102 (2016).
28. I. Ribas, G. F. Porto de Mello, L. D. Ferreira, E. Hébrard, F. Selsis, S. Catalán, A. Garcés, J. D. do Nascimento Jr., J. R. de Medeiros, Evolution of the solar activity over time and effects on planetary atmospheres. II. κ^1 Ceti, an analog of the sun when life arose on earth. *Astrophys. J.* **714**, 384–395 (2010).
29. A. Segura, J. F. Kasting, V. Meadows, M. Cohen, J. Scalo, D. Crisp, R. A. H. Butler, G. Tinetti, Biosignatures from Earth-like planets around M dwarfs. *Astrobiology* **5**, 706–725 (2005).
30. S. Rugheimer, L. Kaltenegger, A. Zsom, A. Segura, D. D. Sasselov, Spectral fingerprints of Earth-like planets around FGK stars. *Astrobiology* **13**, 251–269 (2013).
31. P. B. Rimmer, C. Helling, A chemical kinetics network for lightning and life in planetary atmospheres. *Astrophys. J. Sup. Series* **224**, 9 (2016).
32. F. Gaillard, B. Scaillet, A theoretical framework for volcanic degassing chemistry in a comparative planetology perspective and implications for planetary atmospheres. *Earth Planet. Sci. Lett.* **403**, 307–316 (2014).
33. R. Hu, S. Seager, Photochemistry in terrestrial exoplanet atmospheres. III. Photochemistry and thermochemistry in thick atmospheres on super Earths and mini Neptunes. *Astrophys. J.* **784**, 63 (2014).
34. O. B. Toon, C. P. McKay, T. P. Ackerman, K. Santhanam, Rapid calculation of radiative heating rates and photodissociation rates in inhomogeneous multiple scattering atmospheres. *J. Geophys. Res. Atmos.* **94**, 16287–16301 (1989).
35. M. C. Sauer, R. A. Crowell, I. A. Shkrob, Electron photodetachment from aqueous anions. 1. Quantum yields for generation of hydrated electron by 193 and 248 nm laser photoexcitation of miscellaneous inorganic anions. *J. Phys. Chem. A* **108**, 5490–5502 (2004).

36. S. L. Hawley, B. R. Pettersen, The great flare of 1985 April 12 on AD Leonis. *Astrophys. J.* **378**, 725–741 (1991).
37. A. Segura, L. M. Walkowicz, V. Meadows, J. Kasting, S. Hawley, The effect of a strong stellar flare on the atmospheric chemistry of an Earth-like planet orbiting an M dwarf. *Astrobiology* **10**, 751–771 (2010).
38. S. L. Hawley, J. R. A. Davenport, A. F. Kowalski, J. P. Wisniewski, L. Hebb, R. Deitrick, E. J. Hilton, *Kepler* flares. I. Active and inactive M dwarfs. *Astrophys. J.* **797**, 121 (2014).
39. E. J. Hilton, The galactic M dwarf flare rate, thesis, University of Washington (2011).
40. J. R. A. Davenport, S. L. Hawley, L. Hebb, J. P. Wisniewski, A. F. Kowalski, E. C. Johnson, M. Malatesta, J. Peraza, M. Keil, S. M. Silverberg, T. C. Jansen, M. S. Scheffler, J. R. Berdis, D. M. Larsen, E. J. Hilton, *Kepler* flares. II. The temporal morphology of white-light flares on GJ 1243. *Astrophys. J.* **797**, 122 (2014).
41. B. Kirk, K. Conroy, A. Prša, M. Abdul-Masih, A. Kochoska, G. Matijevič, K. Hambleton, T. Barclay, S. Bloemen, T. Boyajian, L. R. Doyle, B. J. Fulton, A. J. Hoekstra, K. Jek, S. R. Kane, V. Kostov, D. Latham, T. Mazeh, J. A. Orosz, J. Pepper, B. Quarles, D. Ragozzine, A. Shporer, J. Southworth, K. Stassun, S. E. Thompson, W. F. Welsh, E. Agol, A. Derekas, J. Devor, D. Fischer, G. Green, J. Gropp, T. Jacobs, C. Johnston, D. M. LaCourse, K. Saetre, H. Schwengeler, J. Toczyski, G. Werner, M. Garrett, J. Gore, A. O. Martinez, I. Spitzer, J. Stevick, P. C. Thomadis, E. H. Vrijmoet, M. Yenawine, N. Batalha, W. Borucki, *Kepler* eclipsing binary stars. VII. The catalog of eclipsing binaries found in the entire *Kepler* data set. *Astron. J.* **151**, 68 (2016).
42. T. D. Morton, S. T. Bryson, J. L. Coughlin, J. F. Rowe, G. Ravichandran, E. A. Petigura, M. R. Haas, N. M. Batalha, False positive probabilities for all *Kepler* objects of interest: 1284 newly validated planets and 428 likely false positives. *Astrophys. J.* **822**, 86 (2016).
43. I. Angelo, J. F. Rowe, S. B. Howell, E. V. Quintana, M. Still, A. W. Mann, B. Burningham, T. Barclay, D. R. Ciardi, D. Huber, S. R. Kane, Kepler-1649b: An exo-Venus in the solar neighborhood. *Astron. J.* **153**, 162 (2017).
44. R. K. Kopparapu, R. Ramirez, J. F. Kasting, V. Eymet, T. D. Robinson, S. Mahadevan, R. C. Terrien, S. Domagal-Goldman, V. Meadows, R. Deshpande, Habitable zones around main-sequence stars: New estimates. *Astrophys. J.* **765**, 131 (2013).
45. R. K. Kopparapu, R. M. Ramirez, J. SchottelKotte, J. F. Kasting, S. Domagal-Goldman, V. Eymet, Habitable zones around main-sequence stars: Dependence on planetary mass. *Astrophys. J. Lett.* **787**, L29 (2014).
46. R. A. B. Bannard, J. H. Ross, Mono- and dipotassium aminomethionate. *Can. J. Chem.* **32**, 49–50 (1954).
47. D. J. Ritson, J. D. Sutherland, Synthesis of aldehydic ribonucleotide and amino acid precursors by photoredox chemistry. *Angew. Chem. Int. Ed.* **52**, 5845–5847 (2013).
48. D. J. Ritson, J. Xu, J. D. Sutherland, Thiophosphate—A versatile prebiotic reagent? *Synlett* **28**, 64–67 (2017).

Acknowledgments: We thank the three referees for helpful comments. P.B.R. thanks K. France and V. Airipitian for help with stellar UV and particle spectra, and P.B.R. and J.S. thank D. Ritson for key insights regarding the hydrogen sulfide chemistry. **Funding:** We thank the Simons Foundation and Kavli Foundation for funding. **Author contributions:** P.B.R. came up with the original idea for the paper, wrote the majority of the paper and portions of Materials and Methods, and performed the analysis of the chemical kinetics and surface UV fluxes. J.X. and P.B.R. performed all the laboratory experiments together, and J.X. performed the NMR analysis and wrote the Supplementary Materials. S.J.T. and P.B.R. measured the UV output of the mercury lamps together, and S.J.T. wrote the Materials and Methods section regarding the UV lamps. E.G. performed the flare analysis and wrote the relevant section in the main text and Materials and Methods. J.D.S. identified the key light and dark reactions to consider. D.Q. identified appropriate criteria for the planets we consider and helped design Fig. 4. Both J.D.S. and D.Q. participated in writing portions of the main text and edited the entire paper for accuracy and clarity. **Competing interests:** The authors declare that they have no competing interests. **Data and materials availability:** All data needed to evaluate the conclusions in the paper are present in the paper and/or the Supplementary Materials. Additional data related to this paper may be requested from the authors.

Submitted 26 October 2017
Accepted 19 June 2018
Published 1 August 2018
10.1126/sciadv.aar3302

Citation: P. B. Rimmer, J. Xu, S. J. Thompson, E. Gillen, J. D. Sutherland, D. Queloz, The origin of RNA precursors on exoplanets. *Sci. Adv.* **4**, eaar3302 (2018).